

Self-referenced measurement of the complete electric field of ultrashort pulses

Pablo Gabolde and Rick Trebino

Georgia Institute of Technology, School of Physics
837 State St NW, Atlanta, GA 30332, USA
Pablo.Gabolde@physics.gatech.edu

<http://www.physics.gatech.edu/gcuo>

Abstract: A self-referenced technique based on digital holography and frequency-resolved optical gating is proposed in order to characterize the complete complex electric field $E(x, y, z, t)$ of a train of ultrashort laser pulses. We apply this technique to pulses generated by a mode-locked Ti:Sapphire oscillator and demonstrate that our device reveals and measures common linear spatio-temporal couplings such as spatial chirp and pulse-front tilt.

©2004 Optical Society of America

OCIS codes: (320.7100) Ultrafast measurements; (090.2880) Holographic interferometry.

References and links

1. S. Akturk, M. Kimmel, P. O'Shea, and R. Trebino, "Measuring spatial chirp in ultrashort pulses using single-shot Frequency-Resolved Optical Gating," *Opt. Express* **11**, 68-78 (2003), <http://www.opticsexpress.org/abstract.cfm?URI=OPEX-11-1-68>.
2. S. Akturk, M. Kimmel, P. O'Shea, and R. Trebino, "Measuring pulse-front tilt in ultrashort pulses using GRENOUILLE," *Opt. Express* **11**, 491-501 (2003), <http://www.opticsexpress.org/abstract.cfm?URI=OPEX-11-5-491>.
3. J. P. Geindre, P. Audebert, A. Rousse, F. Fallières, J. C. Gauthier, A. Mysyrowicz, A. Dos Santos, G. Hamoniaux, and A. Antonetti, "Frequency-domain interferometer for measuring the phase and amplitude of a femtosecond pulse probing a laser-produced plasma," *Opt. Lett.* **19**, 1997-1999 (1997).
4. T. Tanabe, H. Tanabe, Y. Teramura, and F. Kannari, "Spatiotemporal measurements based on spatial spectral interferometry for ultrashort optical pulses shaped by a Fourier pulse shaper," *J. Opt. Soc. Am. B* **19**, 2795-2802 (2002).
5. C. Dorrer and I. A. Walmsley, "Simple linear technique for the measurement of space-time coupling in ultrashort optical pulses," *Opt. Lett.* **27**, (2002).
6. L. Gallmann, G. Steinmeyer, D. H. Sutter, T. Rupp, C. Iaconis, I. A. Walmsley, and U. Keller, "Spatially resolved amplitude and phase characterization of femtosecond optical pulses," *Opt. Lett.* **26**, 96-98 (2001).
7. C. Dorrer, E. M. Kosik, and I. A. Walmsley, "Spatio-temporal characterization of the electric field of ultrashort pulses using two-dimensional shearing interferometry," *Applied Physics B (Lasers and Optics)* **74** [Suppl.], S209-S217 (2002).
8. S. A. Diddams, H. K. Eaton, A. A. Zozulya, and T. S. Clement, "Full-field characterization of femtosecond pulses after nonlinear propagation," *Conference on Lasers and Electro-Optics Paper CFF3* (1998).
9. B. C. Platt and R. Shack, "History and Principles of Shack-Hartmann Wavefront Sensing," *J. Refractive Surg.* **17**, S573-S577 (2001).
10. C. Elster and I. Weingartner, "Solution to the shearing problem," *Appl. Opt.* **38**, 5024-5031 (1999).
11. E. Arons, D. Dilworth, M. Shih, and P. C. Sun, "Use of Fourier synthesis holography to image through inhomogeneities," *Opt. Lett.* **18**, 1852-1854 (1993).
12. P. Almoró, M. Cadatal, W. Garcia, and C. Saloma, "Pulsed full-color digital holography with a hydrogen Raman shifter," *Appl. Opt.* **43**, 2267-2271 (2004).
13. I. Yamaguchi, T. Matsumura, and J.-i. Kato, "Phase-shifting color digital holography," *Opt. Lett.* **27**, 1108-1110 (2002).
14. Z. Liu, M. Centurion, G. Panotopoulos, J. Hong, and D. Psaltis, "Holographic recording of fast events on a CCD camera," *Opt. Lett.* **27**, 22-24 (2002).
15. E. Leith, C. Chen, Y. Chen, D. Dilworth, J. Lopez, J. Rudd, P. C. Sun, J. Valdmánis, and G. Vossler, "Imaging through scattering media with holography," *J. Opt. Soc. Am. A* **9**, 1148-1153 (1992).
16. M. Takeda, H. Ina, and S. Kobayashi, "Fourier-transform method of fringe-pattern analysis for computer-based topography and interferometry," *J. Opt. Soc. Am.* **72**, 156-160 (1982).

17. S. Rivet, L. Canioni, R. Barille, and L. Sarger, "Multidimensional Shearing for Linear and Nonlinear Propagation Analysis.," Ultrafast Optics Conference Paper M20 (2001).
 18. P. O'Shea, M. Kimmel, X. Gu, and R. Trebino, "Highly simplified device for ultra-short measurement," *Opt. Lett.* **26**, 932-934 (2001).
 19. D. Malacara, *Optical Shop Testing* (John Wiley & Sons, 1992).
 20. J. Liang, B. Grimm, S. Goelz, and J. F. Bille, "Objective measurement of wave aberrations of the human eye with the use of a Hartmann-Shack sensor," *J. Opt. Soc. Am. A* **11**, 1949-1957 (1994).
-

1. Introduction

Ultrashort-pulse measurement devices are usually based on a representation of the electric field as a function of time only, and as a result the spatial beam profile is often regarded as an independent measurement. This approach conceals possible couplings between space and frequency, or space and time, although such couplings are commonly used in pulse compressors, stretchers and shapers, and may subsequently appear as distortions in the pulse. Recently, we showed that frequency-resolved optical gating (FROG) can identify first-order spatiotemporal effects, but only in one spatial direction [1, 2]. Similarly, frequency-domain interferometers can be extended to one transverse spatial dimension. When a reference pulse is present, spectral interferometry (SI) may be spatially resolved [3], or it may be coupled with spatial interferometry to preserve the spatial phase information [4]. Variations of SI have also been reported where a shear is introduced in space [5], or in frequency [6], or both [7]. This last device yields a self-referenced measurement of the phase function $\varphi(x, \omega)$. Such measurements have also been reported using a combination of SI and FROG [8]. Currently, however, there does not exist a self-referenced technique that can measure the complete pulse electric field in space and time, $E(x, y, z, t)$.

Rather than extending time-domain techniques into the space domain, we extend space-domain techniques into the time, or rather, frequency, domain. Numerous intensity-and-phase *spatial*-measurement techniques are available for monochromatic beams, such as direct wavefront sensing [9], or lateral shearing interferometry [10]. Digital holography is another versatile spatial-characterization technique. The latter is relatively inexpensive and easy to implement, so that adding another dimension (time or frequency) to the measurement is quite straightforward.

Indeed, digital holographic measurements have been performed at different wavelengths, sequentially [11], or simultaneously, both with continuous-wave and nanosecond-pulsed laser sources [12, 13], or at different times, on the picosecond time scale [14]. In these experiments, however, the phase function was not measured versus frequency, or time, and therefore they do not constitute a complete measurement of the electric field.

In this work we combine a variation of Fourier-synthesis digital holography [15] with FROG to achieve true self-referenced four-dimensional measurements of the field of potentially arbitrary pulses, $E(x, y, z, t)$. We first discuss the theoretical foundations of the method, before applying it to experimental laser pulses with common spatiotemporal couplings, such as spatial chirp and pulse-front tilt.

2. Method

First, because the electric field satisfies the wave equation, we note that it is sufficient to measure it at a given position $z = z_0$ along the propagation axis. Numerical integration, for example, a convolution with the Fresnel kernel $h(x, y) \equiv h_0 \exp[-i\pi(x^2 + y^2)/(\lambda d)]$ when the paraxial approximation holds, can later be used to numerically (back) propagate each monochromatic component by an arbitrary distance d . Therefore it suffices to measure the pulse for only one value of z , and hence we will suppress the z -coordinate in the rest of this work, and write the complex electric field as $\tilde{E}(x, y, \omega) \equiv \sqrt{S(x, y, \omega)} \exp[i\varphi(x, y, \omega)]$. Its

inverse Fourier transform is $E(x, y, t) \equiv \sqrt{I(x, y, t)} \exp[i\phi(x, y, t)]$, which we approximate by a summation over discrete frequencies:

$$E(x, y, t) = \frac{1}{2\pi} \int_{-\infty}^{+\infty} \exp(+i\omega t) \tilde{E}(x, y, \omega) d\omega \approx \frac{1}{2\pi} \sum_k \exp(+i\omega_k t) \tilde{E}(x, y; \omega_k) \delta\omega. \quad (1)$$

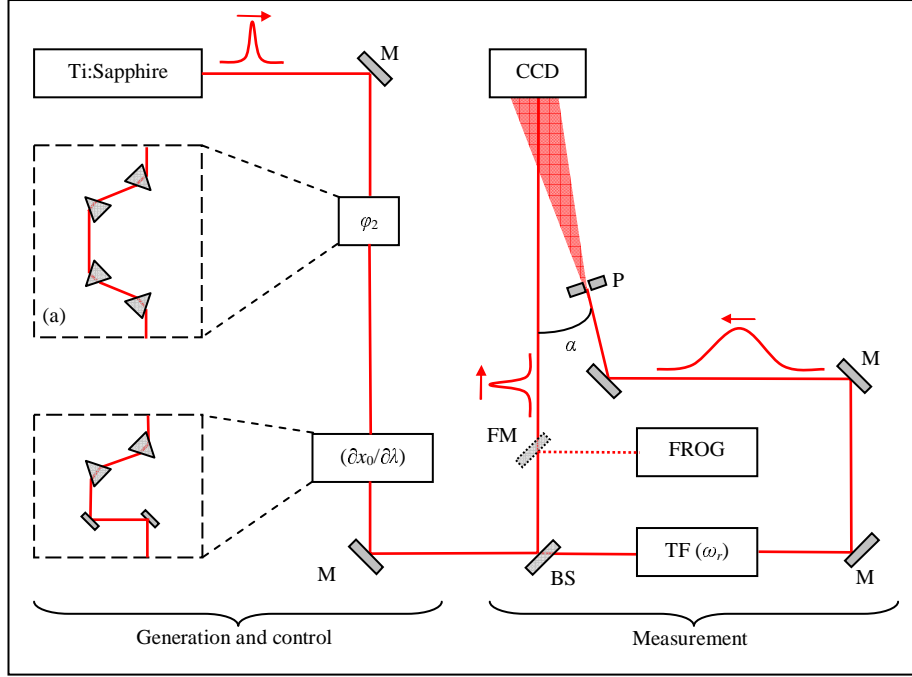


Fig. 1. Schematic of the experiment: (a) 4-prism second-order spectral phase (ϕ_2) control; (b) 2-prism spatial chirp ($\partial x_0 / \partial \lambda$) control; M, mirror; BS, beam-splitter; TF, narrow band-pass filter tuned to frequency ω_r ; P, pinhole; FM, flip-mirror to perform the FROG measurement.

From a single digital holographic experiment one may at the same time isolate and measure an individual complex Fourier component $\tilde{E}(x, y; \omega_k)$. The principle of our experiment is depicted in Fig. 1. A replica of the pulse to be measured is spectrally and spatially filtered by a narrow band-pass filter and a pinhole in order to obtain a quasi-monochromatic, quasi-planar wave in the far field. This wave interferes with the original pulse at an angle α . Note that in this geometry, the original pulse is merely reflected a few times off mirrors and beam-splitters, so that the device does not distort the input pulse. Following the naming convention of holography, we call the tilted, spherical wave the *reference wave* $E_r \equiv \exp(i\omega_r t) \sqrt{R} \exp(ix(\omega_r/c) \sin \alpha)$, and the original pulse the *object wave* $E_o \equiv E(x, y, t) \propto \sum_k \exp(+i\omega_k t) \sqrt{S(x, y; \omega_k)} \exp(i\phi(x, y; \omega_k))$. The resulting interferogram is recorded by a slow detector (a CCD camera), and is usually called a *digital hologram*:

$$\begin{aligned} H(x, y) &\equiv \left\langle |E_r + E_o|^2 \right\rangle_t \\ &= R + \sum_k S(x, y; \omega_k) \\ &\quad + \left[\sqrt{R} \exp(ix(\omega_r/c) \sin \alpha) \sqrt{S(x, y; \omega_r)} \exp(-i\phi(x, y; \omega_r)) + \text{c.c.} \right] \end{aligned} \quad (2)$$

Because of the time averaging $\langle \cdot \rangle_t$ performed by the CCD camera, all the cross-terms present in the expansion of $|E_r + E_o|^2$ vanish, except when $\omega_k = \omega_r$. Therefore, the last term in Eq. (2), located at positive spatial frequency $u_r \equiv (\omega_r / c) \sin \alpha$ contains the intensity and (conjugated) phase $\sqrt{S(x, y; \omega_r)} \exp(-i\varphi(x, y; \omega_r))$ at frequency ω_r , and is easily isolated by a well-established *reconstruction algorithm* based on spatial Fourier transforms [16].

By tuning the band-pass filter to other frequencies, we obtained the discrete set of intensity and phase functions, S and φ , necessary to fully characterize the electric field. But because these measurements are self-referenced, the absolute phase of $\varphi(x, y)$ is lost for each frequency ω_k , i.e., in this typical Fourier-synthesis digital holography experiment [11], the spectral phase of the pulse is not measured. Therefore we perform an additional FROG measurement over a small spatial portion of the beam, to correctly set the relative phase of each Fourier component. A similar rephasing procedure has already been used in frequency-resolved wavefront measurements of ultrashort pulses [17]. It will be successful only if there exists a point (x_0, y_0) in the pulse where the local spectrum $|\tilde{E}(x_0, y_0, \omega)|^2$ contains all the optical frequencies. As long as the beam spatial profile of each frequency extends over this point, this condition is satisfied, for example in the case of moderate amounts of spatial chirp presented below.

3. Experimental details

We measured the spatiotemporal profiles of trains of pulses generated by a mode-locked Ti:Sapphire oscillator with a typical bandwidth of 40 nm. The FROG measurements were performed with a Swamp Optics' GRENOUILLE [18], which had a spectral resolution of 4 nm. This determines the spacing $\delta\omega$ of the holographic measurements, as well as the upper bound of the bandwidth of the band-pass filter. We typically performed 20 measurements to cover the bandwidth of the oscillator (down to 5% of the spectrum peak), using four interference filters that we angle-tuned.

Because two independent functions, $S(x, y)$ and $\varphi(x, y)$, are extracted from a single real-valued hologram $H(x, y)$, a loss of spatial resolution is unavoidable. When no additional frame is recorded to subtract the low spatial frequency term $R + \sum S(x, y; \omega_k)$, the optimal effective resolution is on the order of three times the pitch of the camera. From a 13- μm -pitch camera, we obtained a resolution of 50 μm . From an experimental point of view, however, the low spatial frequency term is quite useful. By application of Parseval's theorem,

$$\sum_k S(x, y; \omega_k) \delta\omega \simeq \int_{-\infty}^{+\infty} I(x, y, t) dt \propto \langle I(x, y, t) \rangle_t. \quad (3)$$

Thus it appears that the second term in Eq. (2), centered at zero spatial frequency, can also be isolated by the reconstruction algorithm, and may be used to measure the time-averaged intensity of the *entire* pulse. The location of each frequency component can thereafter be measured with respect to center of the pulse intensity $\langle I(x, y, t) \rangle_t$, making the device much more tolerant to misalignment as the band-pass filter is tuned.

Also, we would like to point out that it is unrealistic to approximate the reference wave in our configuration as a tilted plane wave. No matter how large the distance L from the pinhole to the camera, the reference wave will manifest a curved wave-front in addition to the tilt. A more precise approximation should therefore be $E_r = \exp(i\omega_r t) \sqrt{R} \exp[ix(\omega_r / c) \sin \alpha + i(x^2 + y^2)\omega_r / (2Lc)]$. Thus the reconstruction algorithm will yield $\sqrt{S(x, y; \omega_r)} \exp[i\pi(x^2 + y^2)\omega_r / (2Lc) - i\varphi(x, y; \omega_r)]$. The phase is contaminated by a pure quadratic term, which is easily removed by calculating the projection of the measured phase $\varphi_m(x, y; \omega_r) \equiv \pi(x^2 + y^2)\omega_r / (2Lc) - \varphi(x, y; \omega_r)$ into the Zernike polynomial $Z_5 \equiv 2(x^2 + y^2) - 1$, and subtracting that term numerically [19, 20]. The advantage

of using a pinhole, compared to, say, a telescope with a large magnification, is that the former creates known intensity and phase reference profiles with minimal aberrations.

4. Experiments with couplings between space and frequency

To test our method, we generated pulses that exhibited a coupling between space and frequency, i.e., whose electric field cannot be factored as $\vec{E}(x, y, \omega) = f(x, y)g(\omega)$. This happens when cross terms $x\omega$ or $y\omega$ are present in the intensity $S(x, y, \omega)$, because of *spatial chirp*, or in the phase $\phi(x, y, \omega)$, because of *angular dispersion*. We studied spatial chirp because an independent measurement was readily available in this case: a spatially-resolved spectrum is a measurement of $S(x, \omega)$, and therefore of spatial chirp along x .

Experimentally we introduced spatial chirp (without angular dispersion) in the beam with a pair of prisms in the arrangement shown in Fig. 1 (b). This results in a quasi linear variation of wavelength with position, at least over the bandwidth of the oscillator.

We measured spatial chirp in two different ways: beam center position versus frequency (or wavelength), $x_0(\lambda)$ and $y_0(\lambda)$; and average frequency (or wavelength) at a fixed position, $\lambda_0(x, y)$. The change of the beam center position with wavelength is clearly illustrated in Fig. 2, which also demonstrates the usefulness of the low-spatial-frequency term $\langle I(x, y, t) \rangle_t$ as a spatial reference. Our measurement matched very well the one obtained from a spatially-resolved spectrum.

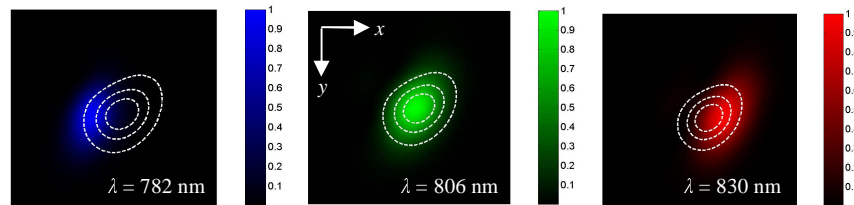


Fig. 2. Plots of the intensity $S(x, y; \omega_k)$ of three spectral components, for ω_k corresponding to 782 nm, 806 nm and 830. The color scales represent the normalized intensities, and the dotted white lines are contour plots of the entire pulse intensity. This pulse exhibits a clear spatial chirp ($\partial x_0 / \partial \lambda$).

5. Experiments with couplings between space and time

In the (x, y, t) domain, cross-terms xt or yt represent *pulse-front tilt* if present in the intensity term $I(x, y, t)$, and spatial chirp if present in the phase term $\phi(x, y, t)$. For pulses without focusing or angular dispersion, the (x, y, t) domain provides a very convenient way of displaying the complex electric field because the phase (derivative) yields the instantaneous wavelength $\lambda(x, y, t) \equiv 2\pi c[\partial\phi(x, y, t)/\partial t]^{-1}$. Quite conveniently, variations of $\lambda(x, y, t)$ with position reveal spatial chirp, and variations with time reveal temporal chirp, while a tilt in the shape of $I(x, y, t)$ is a signature of pulse-front tilt. Therefore, a colored surface plot (see Fig. 3) can be used to display the complete 2-D (x, t) experimental profile of the complex electric field of well-collimated laser pulses (the $\partial/\partial t$ operator acting on the phase function removes time-independent spatial effects such as focusing).

On Fig. 4, we show an experimental 3-D (x, y, t) intensity-and-wavelength profile in the form of a movie, so that space and time naturally represent the spatial and temporal evolution of an ultrashort pulse, respectively.

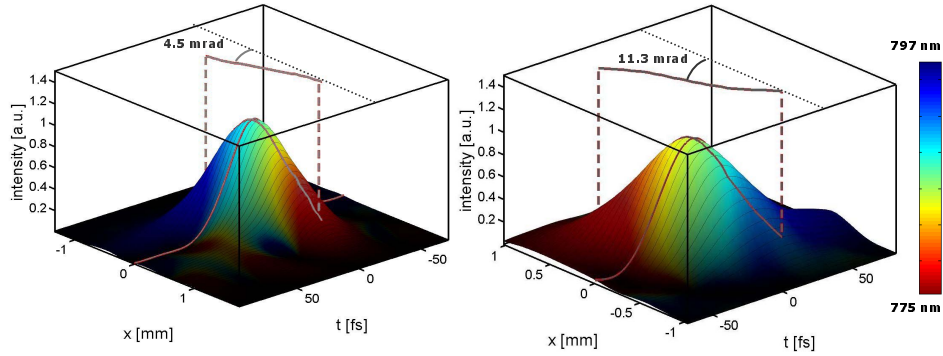


Fig. 3. Profiles in the (x,t) domain of two ultrashort pulses. Both the vertical axis and brightness represent the intensity $I(x,t)$, while colors represent the temporal derivative of the phase $\partial\phi(x,t)/\partial t$, converted to instantaneous wavelength. The solid gray lines that are projected onto the top of each cube correspond to the pulse front $t_0(x)$. The angle of these lines with respect to a reference pulse-front (black dotted line) is a direct measurement of pulse-front tilt, measured in space (left: 4.5 mrad, right: 11.3 mrad).

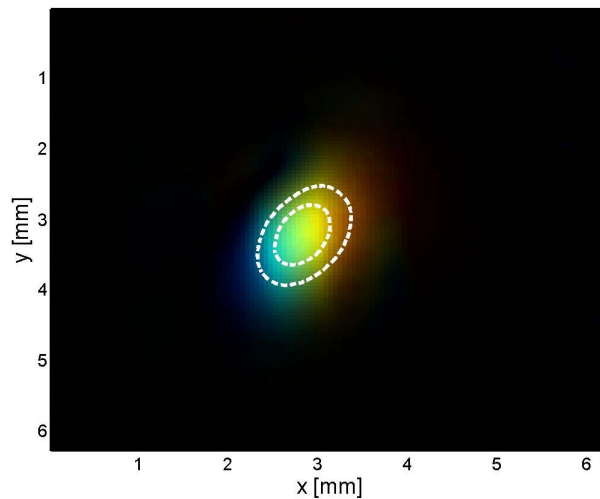


Fig. 4. (3.1 MB) Time-resolved intensity-and-phase measurement of the electric field of an ultrashort pulse. Brightness represents the intensity (dark is zero), and color the instantaneous wavelength (blue is 775 nm, red is 797 nm). To help visualize pulse-front tilt, a contour plot of the intensity has been superimposed (dotted white lines). Note also the presence of spatial chirp and temporal chirp.

5. Conclusion

We have presented a general method to measure the complete complex the electric field of a train of ultrashort pulses, with a resolution of $\delta x \times \delta y \times \delta \lambda = 50 \mu\text{m} \times 50 \mu\text{m} \times 4 \text{nm}$, and a frame size of $100 \times 100 \times 50$. We have tested this method with pulses exhibiting spatial chirp and pulse-front tilt. We have chosen to use digital off-axis holography in conjunction with FROG, but other combinations of amplitude-and-phase spatial and temporal characterization techniques may be employed.

Because we do not make any assumption about the form of the electric field, either in the spatial or temporal domain, the presented technique is naturally sensitive to higher-order

spatiotemporal profiles, and might even be used as the basis for a comprehensive intensity-and-phase spatiotemporal imaging device.

A limitation of the configuration that we have presented is that it requires a train of identical pulses to be generated while the band-pass filter is tuned to different frequencies. However, at high intensity, single-shot operation might be achieved by multiple amplitude division, at the cost of multiple beam-splitting optics. A more practical solution, especially at moderate intensities, would be to use angular-multiplexing, in the fashion of Liu and coworkers [14], at the cost of a reduced spatial resolution.